Optics Letters

Scattering of light by a large, densely packed agglomerate of small silica spheres

T. Väisänen,[1,*] J. Markkanen,[2] E. Hadamcik,[3] J.-B. Renard,[4] J. Lasue,[5] A. C. Levasseur-Regourd,[6] J. Blum,[7] and K. Muinonen[1,8]

[1]Department of Physics, University of Helsinki, P.O. Box 64, Gustaf Hällströmin katu 2, Helsinki FI-00014, Finland
[2]Max Planck Institute for Solar System Research, Justus-von-Liebig-Weg 3, 37077 Göttingen, Germany
[3]LATMOS/IPSL, UVSQ Université Paris-Saclay, Sorbonne Université, CNRS, Guyancourt, France
[4]LPC2E-CNRS, 3A Avenue de la Recherche Scientifique, 45071 Orléans cedex 2, France
[5]IRAP, Université de Toulouse, CNRS, CNES, UPS, 9 Avenue Colonel Roche, 31400 Toulouse, France
[6]LATMOS, Sorbonne Univ., CNRS, UVSQ, Campus Pierre et Marie Curie, 4 Place Jussieu, 75005 Paris, France
[7]Institut für Geophysik und extraterrestrische Physik, Technische Universität Braunschweig, Mendelssohnstr. 3, 38106 Braunschweig, Germany
[8]Finnish Geospatial Research Institute FGI, National Land Survey of Finland, Geodeetinrinne 2, FI-02430 Masala, Finland
*Corresponding author: timo.h.vaisanen@helsinki.fi

Received 6 November 2019; revised 15 February 2020; accepted 16 February 2020; posted 18 February 2020 (Doc. ID 382240); published 17 March 2020

We model the measured phase function and degree of linear polarization of a macroscopic agglomerate made of micrometer-scale silica spheres using the methodology of multiple scattering. In the laboratory work, the agglomerate is produced ballistically, characterized by scanning electron microscopy, and measured with the PROGRA^2 instrument to obtain the light scattering properties. The model phase function and degree of polarization are in satisfactory agreement with the experimental data. To our best knowledge, this is the first time the degree of linear polarization has been modeled well for a large, densely packed agglomerate composed of small particles with known sizes and shapes. The study emphasizes the relevance of the degree of linear polarization and gives insights into the effects of particle aggregation on the scattering characteristics.

https://doi.org/10.1364/OL.382240

Scattering and absorption of light by a particulate medium provide information about the physical properties of the medium and its particles. Computing scattering by a medium with millions of particles is a challenging problem due to the computational complexity. Numerical methods that solve Maxwell's equations exactly in the asymptotic sense, e.g., the fast superposition T-matrix method (FaSTMM, [1]), are limited to media typically smaller than some tens of wavelengths. Thus, approximations have been formulated to simulate scattering by dense particulate media such as snow [dense media radiative transfer (DMRT)] [2] and planetary regoliths [3,4]. One of the most recent approximations is radiative transfer with reciprocal transactions (R^2T^2). It has been shown to extend the applicability of radiative transfer to the dense medium [5–7] by comparing the R^2T^2 computations to the computations with the FaSTMM and radiative transfer with coherent backscattering methods (RT-CB). In comparison, the FaSTMM required around 600 days in serial CPU time to compute ensemble-averaged light scattering characteristics from a dense random medium made of around 31,000 particles, whereas the entire R^2T^2 procedure took only seven days [5].

The R^2T^2 has been used to model the nucleus and dust particles in the coma of Comet 67 P/Churyumov–Gerasimenko [8,9], as well as a levitating analog sample [10]. Here, we use the R^2T^2 to reproduce computationally the light scattering from a centimeter-sized silica sample, measured with the PROGRA^2 instrument [11–13]. The sample had controlled physical parameters, such as the particle size distribution, shape, and total volume fraction of $v = 0.15$ [14]. From scanning electron microscope (SEM) images (Fig. 1), the particles were verified to be mostly spherical, and their radii were found to follow a Gaussian size distribution $\mathcal{N}(0.725\ [\mu m], 0.03\ [\mu m])$ [11]. In addition, the light scattering characteristics of the powder that was used to prepare the agglomerate were measured for levitating particles with the PROGRA^2 instrument. The refractive index of the material was then derived by fitting Lorenz–Mie light scattering characteristics to the measured characteristics [11]. In order to computationally model the light scattering characteristics of the sample, we start by examining the determination of the refractive index from the same measurements.

First, volume elements of radius $R = 1.0\ \mu m$ are generated using spherical particles so that the centers of the spheres are within the volume elements. The volume elements are culled from large periodic boxes packed to the volume fraction of 55% with the spheres whose size distribution obeys $\mathcal{N}(0.725\ [\mu m], 0.03\ [\mu m])$. The small volume elements mimic small clusters of levitating particles because some of the particles are clustered or even sintered together (see Fig. 2 in Ref. [11]). The ensemble-averaged light scattering characteristics of the volume elements are then solved by using the FaSTMM by varying the

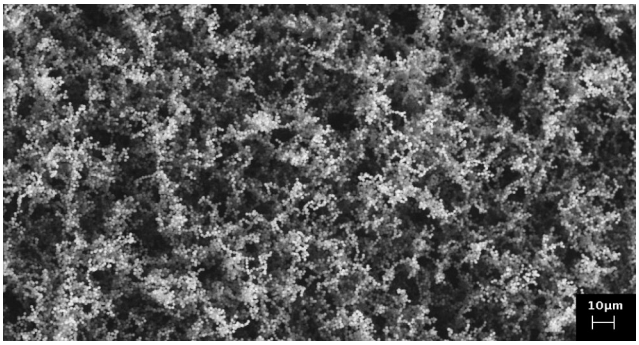

Fig. 1. Scanning electron microscope image of the SiO_2 agglomerate sample. More images, including those of the entire cm-scale sample, are available in Refs. [11,12,14].

complex refractive index. The results and the measurements are compared in Fig. 2, which shows the phase function (scattering matrix element S_{11} [15]) normalized at a 90° scattering angle (spherical polar angle measured from the forward direction) and the degree of linear polarization (scattering matrix element ratio $-S_{12}/S_{11}$ [15]). The determination of the refractive index is difficult because most of the features are hard to match, especially with the phase functions. By comparing the degree of linear polarization near the forward and backward scattering directions, the simulated values are seen to be closer to the measured values near the forward direction. The most notable feature is the missing positive polarization near 150°. The refractive index $m = 1.48 + i10^{-5}$ is chosen because it produces a match with the distinctive feature found near 20° in the measurements of the polarization. In Ref. [11], the refractive index was determined to be $m = 1.48 + i10^{-4}$ for the wavelength of $\lambda = 632.8$ nm with Lorenz–Mie theory, and the results are similar to those in Fig. 2 (see Fig. 10 in Ref. [11]). In comparison, the manufacturer of the silica spheres reported the refractive index of $m = 1.5$. In different measurements made for larger spheres of the same material, the refractive index of $1.30 + i0.08$ was determined for the material, attributed to the porosities reported by the manufacturer [12]. Figure 2 and the work in Ref. [11] are also consistent with the work in Ref. [16], in which agglomerates of different sizes, consisting of the silica spheres with $m = 1.48$ and radius $r = 750$ nm, were measured and simulated with $\lambda = 680$ nm. In Ref. [16], they also reported the missing positive polarization near 150° in their simulations, although the measurements showed a strong positive polarization signature there. They attributed the difference to particle inhomogeneities [17].

The agglomerate can now be modeled with the R^2T^2. The R^2T^2 is a radiative transfer method that is extended to work with dense random particulate media by incorporating so-called incoherent scattering in the frequency domain [18–22]. The incoherent electric field $\mathbf{E}^{sca,ic}$ can be extracted by subtracting the ensemble-averaged total scattered field or coherent field $\mathbf{E}^{sca,c}$ from the scattered field $\mathbf{E}^{sca}$. In the R^2T^2, the single particles are replaced with the incoherent volume elements [7]. The volume elements are generated in the same way as mentioned above, but in order to utilize larger numbers of particles, the size of the volume element is chosen to be $R = 3$ μm. Two different volume fractions are treated here, i.e., $v = 0.15$ and $v = 0.55$. The scattered incoherent electric fields of the volume elements

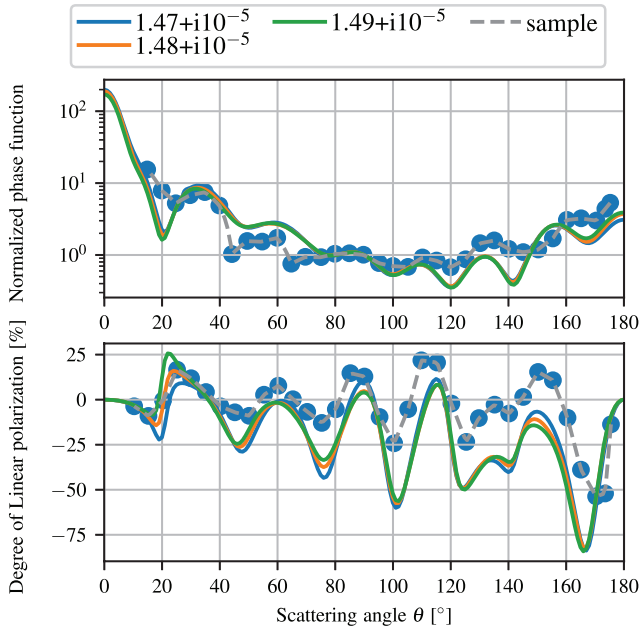

Fig. 2. Comparison of normalized phase function (at 90°) and the degree of linear polarization for levitating particles (measurements, bullets) and small clusters of spherical particles with varying refractive indices (computations, solid lines). Empirical phase function and degree of polarization are also depicted (dashed line).

are then solved using semi-analytical methods such as the FaSTMM, which can be used to generate the input (extinction mean free path length, albedo, effective refractive indices, and incoherent scattering matrix) required for the R^2T^2.

Here, we follow the procedure from [8] in which the R^2T^2 is approximated with the ray tracer SIRIS [7,23,24] which has geometric optics capabilities. SIRIS can be used to model differently shaped diffusely scattering media, but does not have the coherent backscattering capability. In order to create a planar agglomerate for the simulation, the diffuse geometries in SIRIS are approximated by large sphere-like meshes (mean radius $R \approx 2$ mm) that are illuminated by a narrow beam ($R_{beam} = 0.2$ mm) constrained into the center of the medium. Thereby, the global scale structure of the mesh will not affect the simulation, but still, the simulation continues to take into account the local scale surface structures. The final output is smoothened by ensemble averaging using the simulation data from multiple runs of SIRIS that had different geometries as input. Three completely different geometries are used: a sphere, a Gaussian random sphere (GRS) [25], and a sphere with the inner structure of the Gaussian random field (GRFS, Fig. 3). The GRFS is obtained by carving a spherical volume from a sample of Gaussian field [26] and converting the field data to a triangulated mesh with the marching cubes algorithm [27]. The inner parts of the GRFS ($R_{inner} = 1$ mm) are converted to a solid sphere in favor of reducing the triangle count and speeding up the computation. The Gaussian random field has been applied to light scattering problems before, e.g., in Refs. [28,29]. The longest task would take around $3.5 + 27$ days (4 million rays) to create input and finish the ray tracing with a single core. The computations and measurements are shown in Fig. 4, which contains the phase function (normalized in terms of integrated area) and the degree of linear polarization

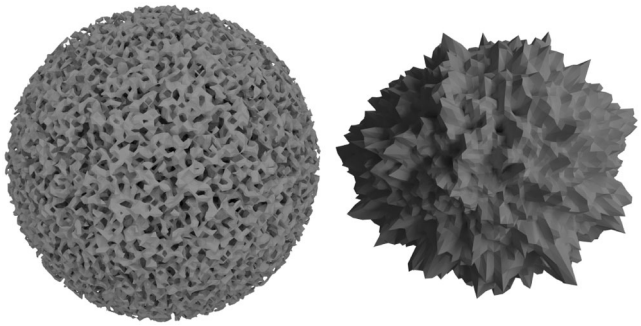

Fig. 3. Samples of Gaussian random field (left) and Gaussian random sphere geometries (right). Their surface elements are invoked as models for the measurement sample in Fig. 4.

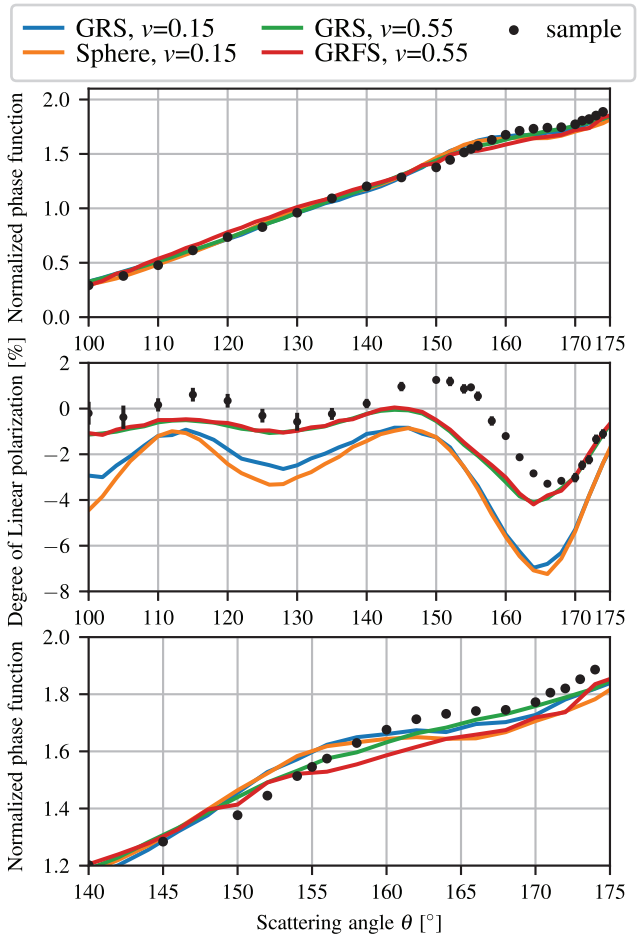

Fig. 4. Measured and modeled light scattering characteristics of the agglomerate. The refractive index is $m = 1.48 + i10^{-5}$, while the volume fraction and the shape of the media are varied. The measurements include the error bars.

as a function of the scattering angle. Due to the fact that the measured data range from 100° to 175°, thus not reaching the angles near backscattering, the coherent backscattering modeling is omitted.

By looking at only the overall phase function in Fig. 4, we could argue that the $v = 0.15$ volume element produces a good match with the measurement. The phase function has a distinctive bump at 155°, which in the measurement is near 160°. The level of backscattering is slightly lower than that in the measurements, but this can be mitigated with the increase in the shadowing effect [4]. It is the degree of linear polarization that reveals a difference between the simulation and the measurement. The polarization shows the same 5° shift as the phase function (Fig. 2 shows the same shift), and there is a uniform difference of around 2%–4%. The match in the degree of linear polarization is improved by using the $v = 0.55$ volume element, and the difference is only 1%–3%. However, the 5° shift to the left is still present. For the $v = 0.55$ volume element, the phase function is also flatter than that for the $v = 0.15$ volume element. This is seen in the loss of the distinctive bump near $\theta \approx 160°$, which is more prominent with the GRFS samples. In general, similar results are obtained with the GRS and GRFS models, which shows that small changes in the geometry do not impact the results substantially. Thus, the focus can be on the properties of the particles. For changes due to the overall shape of the finite medium, compare "Sphere, $v = 0.15$" with "GRS, $v = 0.15$" in Fig. 4.

The use of the $v = 0.55$ volume element improves the modeling. The dense volume element does not contradict the measured volume fraction of $v = 0.15$ because the SEM image (see Fig. 1 or Fig. 4 in Ref. [11]) shows that the spheres have formed threads of clumps that are closely connected probably by sintering, forming high-density localities separated by empty spaces. Moreover, the particles in the $v = 0.15$ volume elements were uniformly placed, whereas Fig. 1 shows aggregated structures. Modeling the aggregated structures can introduce the bump near $\theta \approx 160°$ due to the introduction of the sparse regions to the dense volume element, but can lower the negative polarization at $\theta \approx 165°$. The dense volume element is still insufficient, as seen in Fig. 2 where prominent positive polarization is again missing.

It is interesting to notice that most of the features seen in the scattering characteristics of the agglomerate are also visible for the levitating sample (cf. measurements in Figs. 2 and 4). The same can be concluded in the case of the computations: the features are aligned. This means that the features are consistent between the measurements and the computation, and by achieving a better match with the scattering characteristics of the levitating sample, the results for the agglomerate should improve. In order to test this, we generated an empirical volume element using the measured scattering matrix elements of the levitating sample M^l_{11} and $-M^l_{12}/M^l_{11}$ and using the computed matrix elements for the $v = 0.55$ volume element S^v_{11} and $-S^v_{12}/S^v_{11}$. First, the empirical volume element phase function S^{ve}_{11} is obtained by scaling M^l_{11} with the coefficient S^v_{11}/S^s_{11}, where S^s_{11} refers to the average phase function of simulated levitating particles: $S^{ve}_{11} \propto M^l_{11} S^v_{11}/S^s_{11}$. Then, a scaling factor $\beta \approx 0.32$ for $-M^l_{12}/M^l_{11}$ is found by minimizing the root-mean-square difference between $-\beta S^s_{12}/S^s_{11}$ and $-S^v_{12}/S^v_{11}$. The resulting degree of linear polarization for the empirical volume element is then $-S^{ve}_{12}/S^{ve}_{11} = -\beta M^l_{12}/M^l_{11}$. The other matrix elements are assumed to be zero except for $S^{ve}_{21} = S^{ve}_{12}$, $S^{ve}_{22} = S^{ve}_{11}$, and $S^{ve}_{33} = S^{ve}_{44} = \pm S^{ve}_{11}\sqrt{1 - [S^{ve}_{12}/S^{ve}_{11}]^2}$ (positive sign for scattering angles $< 90°$). The empirical scattering matrix is then used as input for R^2T^2, by keeping the rest of the volume element parameters unchanged. The results in Fig. 5

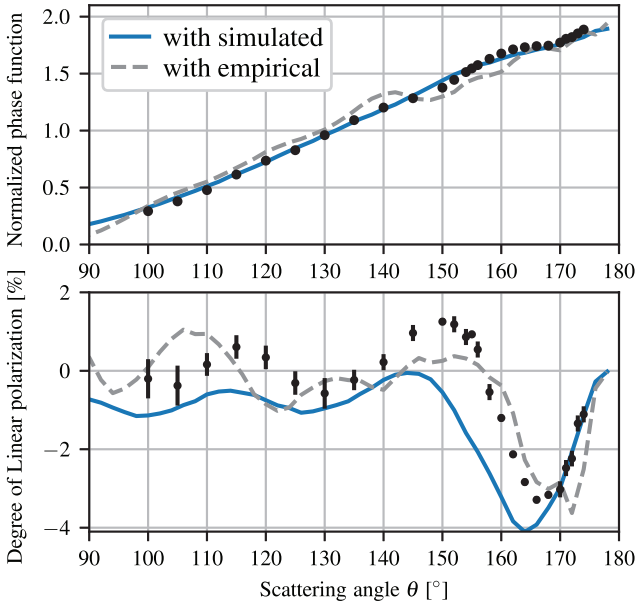

Fig. 5. Measured and modeled light scattering characteristics of the agglomerate with different volume elements. The result with the simulated volume element is the "$v = 0.55$, GRS" case in Fig. 4.

show that the empirical volume element removes the differences due to the original simulation, such as the 5° shift and the missing positive polarization. The results indicate that once correct modeling is obtained for the levitating sample (Fig. 2), the agglomerate scattering characteristics will also be modeled correctly.

Even though there are differences between the measurements and the computational results, the examination of the input and the results shows that the modeling and the measurements are consistent. By improving the characterization of the levitating particles, a better match would be obtained with the R^2T^2 for the agglomerate. In a future study, improved modeling for the levitating particles could involve sintered particles, small aggregates, or particles with other kinds of deformations, and a distribution of the refractive indices. Simulating the entire volume element for the R^2T^2 with irregular particles is computationally challenging but not impossible, especially when modeling the scattering by the levitating particles at the same time. The present results are promising. With the empirical volume element (Fig. 5), the normalized root-mean-square error in modeling the agglomerate phase function is less than 7%, and the degree of linear polarization is within 1.5% of the measurements. With the simulated volume element, the respective numbers are 2.5% and 3%. The study stresses the importance of sample characterization in light scattering measurements. Finally, the study emphasizes the importance of polarization: the physical characteristics are hard to retrieve from the phase function only.

Funding. Academy of Finland (1325805); Deutsches Zentrum für Luft- und Raumfahrt (50WM1236, 50WM1536, 50WM1846); Centre National d'Etudes Spatiales; European Research Council (757390).

Acknowledgment. Computational resources were provided by CSC–IT Centre for Science Ltd., Finland, and Finnish Grid and Cloud Infrastructure (urn:nbn:fi:research-infras-2016072533).

Disclosures. The authors declare no conflicts of interest.

REFERENCES

1. J. Markkanen and A. J. Yuffa, J. Quant. Spectrosc. Radiat. Transfer **189**, 181 (2017).
2. L. Tsang, C.-T. Chen, A. T. C. Chang, J. Guo, and K.-H. Ding, Radio Sci. **35**, 731 (2000).
3. B. Hapke, J. Geophys. Res. **86**, 3039 (1981).
4. K. Lumme, J. I. Peltoniemi, and W. M. Irvine, Transport Theory Statist. Phys. **19**, 317 (1990).
5. K. Muinonen, J. Markkanen, T. Väisänen, J. Peltoniemi, and A. Penttilä, Opt. Lett. **43**, 683 (2018).
6. J. Markkanen, T. Väisänen, A. Penttilä, and K. Muinonen, Opt. Lett. **43**, 2925 (2018).
7. T. Väisänen, J. Markkanen, A. Penttilä, and K. Muinonen, PLoS ONE **14**, e0210155 (2019).
8. J. Markkanen, J. Agarwal, T. Väisänen, A. Penttilä, and K. Muinonen, Astrophys. J. Lett. **868**, L16 (2018).
9. J. Markkanen and J. Agarwal, Astron. Astrophys. **631**, A164 (2019).
10. K. Muinonen, T. Väisänen, J. Martikainen, J. Markkanen, A. Penttilä, M. Gritsevich, J. Peltoniemi, J. Blum, J. Herranen, G. Videen, G. Maconi, P. Helander, A. Salmi, I. Kassamakov, and E. Haeggström, J. Vis. Exp. **149**, e59607 (2019).
11. E. Hadamcik, J.-B. Renard, J. Lasue, A. C. Levasseur-Regourd, J. Blum, and R. Schraepler, J. Quant. Spectrosc. Radiat. Transfer **106**, 74 (2007).
12. E. Hadamcik, J.-B. Renard, A. C. Levasseur-Regourd, J. Lasue, G. Alcouffe, and M. Francis, J. Quant. Spectrosc. Radiat. Transfer **110**, 1755 (2009).
13. A. C. Levasseur-Regourd, J.-B. Renard, Y. Shkuratov, and E. Hadamcik, in *Polarimetry of Stars and Planetary Systems*, L. Kolokolova, J. Hough, and A. C. Levasseur-Regourd, eds. (Cambridge University, 2015), pp. 62–80.
14. J. Blum and R. Schräpler, Phys. Rev. Lett. **93**, 115503 (2004).
15. C. F. Bohren and D. R. Huffman, *Absorption and Scattering of Light by Small Particles* (Wiley, 1983).
16. G. Wurm, H. Relke, J. Dorschner, and O. Krauß, J. Quant. Spectrosc. Radiat. Transfer **89**, 371 (2004).
17. G. Wurm, H. Relke, and J. Dorschner, Astrophys. J. **595**, 891 (2003).
18. A. Ishimaru, *Wave Propagation and Scattering in Random Media, An IEEE OUP Classic Reissue* (Wiley, 1999).
19. L. Tsang, J. Kong, and R. Shin, *Theory of Microwave Remote Sensing*, Wiley Series in Remote Sensing and Image Processing (Wiley, 1985).
20. L. Tsang, C. E. Mandt, and K. H. Ding, Opt. Lett. **17**, 314 (1992).
21. L. M. Zurk, L. Tsang, and D. P. Winebrenner, Radio Sci. **31**, 803 (1996).
22. M. I. Mishchenko, L. D. Travis, and A. A. Lacis, *Multiple Scattering of Light by Particles: Radiative Transfer and Coherent Backscattering* (Cambridge University, 2006).
23. K. Muinonen, T. Nousiainen, H. Lindqvist, O. Muñoz, and G. Videen, J. Quant. Spectrosc. Radiat. Transfer **110**, 1628 (2009).
24. H. Lindqvist, J. Martikainen, J. Räbinä, A. Penttilä, and K. Muinonen, J. Quant. Spectrosc. Radiat. Transfer **217**, 329 (2018).
25. K. Muinonen, T. Nousiainen, P. Fast, K. Lumme, and J. Peltoniemi, J. Quant. Spectrosc. Radiat. Transfer **55**, 577 (1996).
26. S. Müller and L. Schüler, *Geostat-Framework/gstools: Bouncy Blue* (2019).
27. W. E. Lorensen and H. E. Cline, SIGGRAPH Comput. Graph. **21**, 163 (1987).
28. J. I. Peltoniemi, J. Quant. Spectrosc. Radiat. Transfer **50**, 655 (1993).
29. Y. Grynko and Y. Shkuratov, J. Quant. Spectrosc. Radiat. Transfer **78**, 319 (2003).